Chemical Engineering Journal 162 (2010) 901–909

Contents lists available at ScienceDirect

Chemical Engineering Journal

journal homepage: www.elsevier.com/locate/cej

Templated Silica with Increased Surface Area and Expanded Microporosity: Synthesis, Characterization, and Catalytic Application

Chi He[a,b], Qin Li[c], Peng Li[a], Yufei Wang[a], Xinyan Zhang[a], Jie Cheng[a], Zhengping Hao[a,*]

[a] State Key Laboratory of Environmental Chemistry and Ecotoxicology, Research Center for Eco-Environmental Sciences, Chinese Academy of Sciences, Shuangqing Road No. 18, Beijing 100085, China
[b] Key Lab of Urban Environment and Health, Institute of Urban Environment, Chinese Academy of Sciences, Xiamen 361021, China
[c] Department of Chemical Engineering, Curtin University of Technology, Perth, Western Australia 6845, Australia

ARTICLE INFO

Article history:
Received 6 April 2010
Received in revised form 24 June 2010
Accepted 25 June 2010

Keywords:
SBA-15
Micro/mesoporous composite
Highly dispersed Pd
VOCs
Superior activity and stability

ABSTRACT

In this paper, we report a convenient and effective approach to synthesizing mesoporous SBA-15 materials with increased surface area (up to 836.7 cm^3/g) and expanded microporosity (up to 0.22 cm^3/g), where the textural properties of the synthesized materials can be systematically controlled. These micro/mesoporous composite materials exhibit excellent performance in catalysis, adsorption and separation. Moreover, the synthesized materials that supported Pd catalysts obtained through impregnation and grafting approaches were tested to explore their flexibility in toluene elimination. Grafting is an effective method to obtain highly dispersed Pd nanoparticles compared with traditional impregnation approach. The catalyst prepared *via* the grafting procedure possesses higher activity and CO_2 selectivity than that was prepared by impregnation method. Moreover, the catalytic performance of synthesized catalysts can be well sustained during the stability tests. Therefore, these novel Pd-supported catalysts are promising materials for effective removal of some types of volatile organic compounds (VOCs) such as toluene.

1. Introduction

Silica-based ordered mesoporous materials have shown significant potential for being used as catalysts, adsorbents and chemicals/drugs hosts in recent years owing to their high specific surface area and narrow pore size distribution [1–3]. However, compared with microporous zeolites crystals, as-prepared mesoporous silica materials do not possess specific catalytic and adsorption properties such as the uniform acidity, strong adsorption ability and high hydrothermal stability due to the amorphous pore walls and large pore dimensions [4]. One of the strategies to improve is to embed the crystal microporous zeolite within the amorphous pore walls of mesoporous materials [5]. Such a hierarchical micro/mesoporous material in principle should have superior properties on the hydrothermal stability [6,7], capabilities of encapsulating wastes in the micropores, better adsorption property and catalytic efficiency (by improving the diffusion rate for transport in catalytic processes), etc.

The mesoporous SBA-15, which contains micropores within the walls of primary mesopores forming 3D connected pore network, has attracted increasing interests in recent years [8–11]. However, the micropore volume in conventional SBA-15 is rather low (about 0.02 cm^3/g), hence limiting its application. Therefore, the synthesis of SBA-15 with increased micoporosity would be of great interest. Inagaki et al. reported that the micropore volume of SBA-15 can be increased by controlling the TEOS/surfactant ratio in the starting mixture. However, the increase of the micropore volume is at the expense of the specific surface area (typical: 436 m^2/g) [4]. Van Der Voort et al. [12] reported the synthesis of micro- and mesoporous composite molecular sieve with high hydrothermal stability and large micropore volume, whereas most of mesopores over the synthesized materials were blocked. More recently, Vallet-Regi and co-workers [13] synthesized the hexagonally ordered SBA-15 materials with increased surface area and mesoporous volume by adopting HCl and H_3PO_4 mixture solution for the template formation during the synthesis procedures. In addition, the phosphorus species in mesoporous frameworks can act as acid centers in catalysis and biomaterial science [14,15]. However, no change can be observed for the micropore volume. Jaroniec and co-workers [16] reported that the amount of the micropores in SBA-15 is dependent to some extent on the synthesis/aging temperature, i.e., the relative amount of the micropore volume decreases significantly when increasing the synthesis/aging temperature due to the dehydration of EO blocks at higher temperatures. It is a worthwhile effort to synthesize SBA-15 materials with large micropore volume and high surface area. Unfortunately, no such

---

* Corresponding author. Tel.: +86 10 62849194; fax: +86 10 62923564.
E-mail address: zpinghao@rcees.ac.cn (Z. Hao).

1385-8947/$ – see front matter © 2010 Elsevier B.V. All rights reserved.
doi:10.1016/j.cej.2010.06.037

work yet has been reported, maybe because of the technical challenge.

In this work, a convenient and effective approach to synthesis ordered SBA-15 materials with increased surface area and expanded micropore volume was firstly reported. Moreover, the synthesis materials that support Pd catalysts were prepared *via* conventional impregnation method and direct grafting approach, and their activity, selectivity and stability in deep catalytic oxidation of toluene were also comprehensively investigated. To the best of our knowledge, such a systematic study has not been reported. We could anticipate that the synthesized novel materials that supported nanometric Pd catalysts probably possess excellent catalytic performance in volatile organic compounds (VOCs) oxidation elimination, and these micro- and mesoporous combined materials may have extensive applications in catalysis, adsorption and separation.

VOCs are considered as the major contributors to air pollution and are dangerous to human health and the environment [17]. Stringent environmental regulations have been developed and implemented to reduce the VOCs emission [18]. Among all VOCs, BTX (benzene, toluene and xylene) are of particular concern due to their high toxicity for human beings [19–21]. Currently, VOCs catalytic oxidation has been widely investigated over different types of catalysts such as supported noble metals, metal oxides, and mixtures of noble metals and metal oxides [22,23]. Particularly, Pd-loaded catalysts are extensively examined as Pd catalyst is promising for practical applications in hydrocarbons total combustion [24]. Therefore, it is of significant importance to develop effective and highly active catalysts for the total oxidation elimination of VOCs at mild conditions.

2. Material and methods

2.1. Material preparation

The synthesis of hexagonally ordered SBA-15 with increased surface area and expanded microporosity is through the addition of H_3PO_4 and variation of the synthesis conditions, i.e., SiO_2/P123 molar ratio and ageing temperature. Typically, 4 g of Pluronic P123 (nonionic triblock copolymer, $EO_{20}PO_{70}EO_{20}$) was dissolved in an acid solution containing 139 g of H_2O, 14.5 g of HCl (36.5%) and 10.8 g of H_3PO_4 (85%) at 35 °C for 1 h (pH 0.27). Then, different amounts of tetraethyl orthosilicate (TEOS) were added to obtain the following molar composition of SiO_2/P123 = 59, 92, 125 and 152. The resulting mixture was stirred at 35 °C for 20 h and then aged at 80 or 100 °C for 24 h under static condition (Table 1). The recovered solid was extensively washed with deionized water and dried at 100 °C for 12 h in air. Template removal was performed by calcination in air using two successive procedures, i.e., heating at 350 °C for 3 h and then at 550 °C for 4 h. Finally, six modified samples, denoted as HP_x-y (x is the SiO_2/P123 molar ratio and y is the ageing temperature), were prepared.

For comparison, pure SBA-15 was synthesized following the literature procedure [25], i.e., 4 g of P123, 135 g of H_2O, 24 g of HCl and 9.1 ml of TEOS were mixed under stirring at 35 °C for 20 h, and followed by ageing, filtration and calcination. Similarly, template removal was performed by heating at 350 °C for 3 h and then at 550 °C for 4 h, denoted as SBA-15-t. At the same time, conventional SBA-15, using one-step calcination at 550 °C for template removal, was also prepared.

2.2. Catalyst synthesis

1.0 g of the synthesized support (HP_{59}-80, HP_{92}-80 or SBA-15) was suspended in 75 ml of dry toluene under flowing N_2 and then 3.0 ml of 3-aminopropyltrimethoxysilane (APTMS) was added under stirring. The obtained mixture was stirred for another 12 h at room temperature and refluxed at 80 °C for 8 h. The solid was obtained after washing with toluene and then with ethanol intensively to eliminate the physically adsorbed APTMS and toluene. The modified samples after being vacuum-dried at 80 °C for 6 h were labeled as A-HP_{59}-80, A-HP_{92}-80 and A-SBA-15, respectively. To introduce Pd, 1.0 g of A-HP_{59}-80, A-HP_{92}-80 or A-SBA-15 was added into a mixture of H_2O and 7.8 ml of $PdCl_2$ aqueous solution (2.55 mg Pd/ml, $H_2O/PdCl_2$ = 4:1, v/v). And the mixture was then stirred at room temperature for 2 h, dried at 40 °C for 24 h, followed by calcination at 550 °C for 2 h and reduced in a pure H_2 stream (30 ml/min) at 480 °C for 1 h. The obtained catalysts were denoted as GtPd/HP_{59}-80, GtPd/HP_{92}-80 and GtPd/SBA-15, respectively.

For comparison, the Pd-loaded catalyst was also prepared by impregnation method. The porous HP_{92}-80 was impregnated with a $PdCl_2$ aqueous solution and dried at 40 °C for 24 h, followed by calcination at 550 °C for 2 h and reduction in a pure H_2 stream (30 ml/min) at 480 °C for 1 h, and the obtained sample was named as ImPd/HP_{92}-80. The nominal Pd loading of all catalysts were 2.0 wt.%.

Table 1
Physicochemical properties of synthesized materials.

Sample	A_t[a] (°C)	S_{BET}[b] (m^2/g)	D_v[c] (cm^3/g)	S_{mi}[d] (m^2/g)	D_{mi}[e] (cm^3/g)	D_{micro}[f] (%)	D_p[g] (nm)	d_{100}[h] (nm)	a_0[i] (nm)	W[j] (nm)	R_{wd}[k]
SBA-15	100	759.9	1.06	49.4	0.02	1.9	5.62	8.98	10.36	4.74	0.84
SBA-15-t[l]	100	766.2	1.06	102.7	0.05	4.7	5.54	8.97	10.35	4.81	0.86
HP_{59}	100	811.4	1.08	198.2	0.06	5.5	5.69	9.24	10.66	4.97	0.87
HP_{92}	100	823.9	0.99	258	0.12	12.1	5.05	9.36	10.80	5.75	1.13
HP_{59}	80	805.2	0.97	316.3	0.10	10.3	5.11	9.12	10.52	5.41	1.05
HP_{92}	80	836.7	0.92	427.4	0.18	19.5	4.76	9.30	10.73	5.97	1.25
HP_{125}	80	813.4	0.86	431.1	0.20	23.2	3.96	9.28	10.71	6.75	1.64
HP_{152}	80	770.1	0.71	411.3	0.22	30.9	3.82	9.31	10.73	6.91	1.81

[a] Aging temperature.
[b] BET specific surface area.
[c] Total pore volume estimated at P/P_0 = 0.99.
[d] Micropore surface area estimated from the *t*-plot method.
[e] Micropore volume estimated from the *t*-plot method.
[f] Percentage of micropore volume to total pore volume (D_{mi}/D_v).
[g] BJH pore diameter calculated from the desorption branch.
[h] Interplanar spacing of the (1 0 0) plane, calculated by the Bragg's Law.
[i] Lattice parameter, $a_0 = 2 \times d_{100}/\sqrt{3}$.
[j] Wall thickness = $a_0 - D_p$.
[k] The ratio of pore wall thickness to pore diameter (W/D_p).
[l] Template removed by two successive calcination steps.

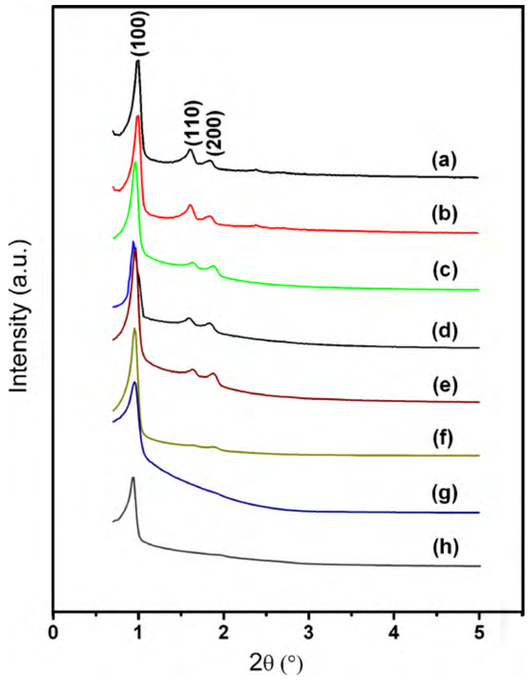

Fig. 1. SA-XRD patterns of (a) SBA-15, (b) SBA-15-t, (c) HP_{59}-100, (d) HP_{92}-100, (e) HP_{59}-80, (f) HP_{92}-80, (g) HP_{125}-80 and (h) HP_{152}-80.

2.3. Characterizations

X-ray diffraction (XRD) patterns were recorded on a PANalytical X'Pert PRO powder diffraction system using Cu Kα radiation ($\lambda = 0.15418$ nm) in the 2θ range of 0.7–5° (scanning rate of 0.5°/min) and 10–80° (scanning rate of 4°/min), respectively. The exact Pd loading in all synthesized samples was determined by inductively coupled plasma optical emission spectroscopy (ICP-OES) on an OPTIMA 2000. The palladium dispersion was assessed by H_2 chemisorption at 25 °C, i.e., the molar ratio of H/Pd [26]. The mean Pd crystallite size was further estimated from the equation: d (nm) = 112/(percentage of Pd exposed) [27], assuming that the Pd crystallites were spherical with a surface atom density of 1.27×10^9 atoms/m^2. N_2 adsorption/desorption isotherms of catalysts at 77 K were collected on a gas sorption analyzer NOVA1200. All samples were degassed under vacuum at 300 °C for 3 h before the measurement. The total pore volume was estimated from the amount of nitrogen adsorbed at a relative pressure (P/P_0) of *ca.* 0.99. The specific surface area (S_{BET}) was calculated using the Brunauer–Emmett–Teller (BET) method and the micropore surface area and micropore volume were estimated by the t-plot method (the surface area of material synthesized at 80 °C may be an approximation [28]). The pore size distribution (PSD) was derived from the desorption branch of the N_2 isotherm using the Barrett–Joyner–Halenda (BJH) method. Thermogravimetric analysis (TGA) was performed on a Setaram Labsys, where *ca.* 10 mg of finely ground sample was heated from 50 to 800 °C at a heating rate of 10 °C/min with air flowing at 30 ml/min. Fourier transform infrared (FT-IR) spectra were recorded using a Bruker Tensor 27 IR spectrometer. Transmission electron microscope (TEM) images were recorded on a Hitachi H-7500 microscope operating at an accelerating voltage of 80 kV. High resolution transmission electron microscope (HRTEM) and scanning transmission electron microscope (STEM) images were recorded on a FEI Tecnai G2 F20 U-TWIN microscope operating at an accelerating voltage of 200 kV. All samples were ground, dispersed in ethanol and deposited on the micro-grids prior to observation. Energy dispersive spectrograph (EDS) was performed on a Hitachi S-3000N for composition analysis of the synthesized catalyst. ^{29}Si CP-MAS/NMR spectra were performed on a Bruker AC-80MHZ spectrometer equipped with a 5 mm BBI detector and a spinning frequency of 5 kHz.

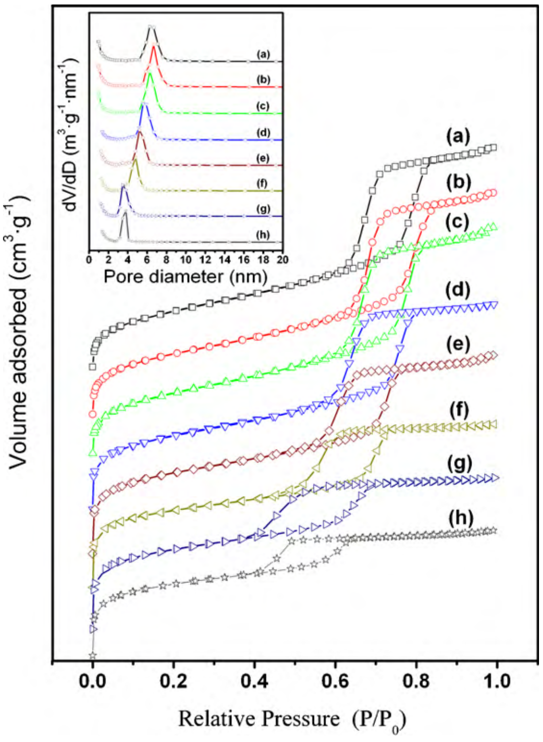

Fig. 2. N_2 adsorption/desorption isotherms and pore size distribution calculated from the desorption branch (insert) of (a) SBA-15, (b) SBA-15-t, (c) HP_{59}-100, (d) HP_{92}-100, (e) HP_{59}-80, (f) HP_{92}-80, (g) HP_{125}-80 and (h) HP_{152}-80.

2.4. Catalytic oxidation activities

All evaluation experiments were performed in a continuous-flow fixed-bed reactor at atmospheric pressure, consisting of a stainless steel tube (6 mm i.d.) that was filled with the catalyst. The VOC-containing gas was generated by bubbling air through the VOC saturator and then further diluted with another air stream before reaching the reaction bed. The temperatures of the catalyst bed and tubular electric furnace were monitored automatically by E-type thermocouples. In each test, 200 mg of the catalyst (40–60 mesh) was placed at the middle of the tube reactor and the total flow rate was kept at 350 ml/min, i.e., gas hourly space velocity (GHSV) of 45,000 h^{-1}, and the O_2 feed concentration was kept at about 21% (v/v). In each test, the catalyst bed temperature was first raised to 130 °C with the feed stream passing and stabilized for 30 min. Then the temperature was increased to the next one at a heating rate of 5 °C/min and stabilized for 20 min prior to online analysis of the effluent gas composition in an Agilent gas chromatograph equipped with an FID and a TCD. VOC concentrations in the feed and effluent streams were determined with the FID after being separated in an AB-GASPRO capillary column, and CO/CO_2 in the effluent stream were separated in a TDX-01 column and their concentrations were determined with the TCD.

3. Results and discussion

3.1. Structural and textural properties of modified SBA-15

The small-angle XRD (SA-XRD) patterns of synthesized SBA-15 materials in the 2θ range of 0.7–5° are shown in Fig. 1. All samples exhibit one intense peak at 0.8–1.0° along with two weak peaks at 1.4–2.0°, which can be assigned to the (1 0 0), (1 1 0), and (2 0 0) reflections of the two-dimensional hexagonal mesostructure with a space group of *p*6*mm* symmetry [13]. The related structure parameters of all samples are summarized in Table 1. By carefully comparing the patterns in Fig. 1, we can observe that all peaks shift slightly to lower angles after H_3PO_4 addition, corresponding to a slight increase of d_{100} and a_0, as listed in Table 1. This shift suggested that the frameworks of the modified materials are slightly enlarged during the synthesis process [10,29]. In addition, it is noted that the ordered structures remained although the intensities of diffraction peaks decreased to some extent when increasing the $SiO_2/P123$ ratios.

Fig. 2 shows the N_2 adsorption/desorption isotherms and the BJH pore size distribution calculated from the desorption branch (insert) for all synthesized materials. All samples possess the type IV isotherms, typical characteristic of mesoporous materials [10]. Both SBA-15 and SBA-15-t show H1 type hysteresis loop according to the IUPAC classification [30], which indicated the two-dimensional *p*6*mm* structure formed by open cylindrical mesopores. The adsorption isotherms of all modified materials exhibit sharp increases at $P/P_0 < 0.1$ and $P/P_0 = 0.4–0.85$, as shown in Fig. 2(c)–(h). The first increase ($P/P_0 < 0.1$) is due to the multilayer adsorption on the surface (characteristic of microporous materials), while the second increase ($P/P_0 = 0.4–0.85$) arises from the capillary condensation in the mesopores with N_2 adsorbed on the inner surface [4]. The ratio of the first to second feature increases with the raise of the $SiO_2/P123$ ratios, suggesting that the micropore volume increased. In addition, the hysteresis loops of HP_{92}-100, HP_{59}-80, HP_{92}-80, HP_{125}-80 and HP_{152}-80 become smaller, and the position of the step shifts towards lower relative pressure in the range of 0.4–0.8 (Fig. 2(d)–(h)), indicating that smaller pore sizes were formed. On the other hand, we can draw the following conclusions from the data in Table 1: firstly, the method employed for template removal plays an important role in the micropore properties of the final materials. During the first stage, the relatively low calcination temperature may have prevented the silica matrix from shrinking, and hence maintained the original size and volume of the micro- and mesopores [31]. Thus, the two successive calcination procedures were adopted in this work. Secondly, the phosphate molecules located among the triblock copolymer micelles may have changed the ionic strength and pH of the environment, and hence induced a different silica–surfactant interaction type (result in materials with different textural properties). Herein, the use of HCl and H_3PO_4 mixed aqueous solution possibly has acted as “catalyst” during the template formation process resulting in an obvious increase in the surface area of the obtained materials (>770 m^2/g) [13,32], while there was a slight increase in micropore volume (from 0.05 to 0.06 cm^3/g). Thirdly, the micropore volume in the final materials changed systematically with variation of $SiO_2/P123$ ratio due to the structure changes of siloxane network in the pore walls [33], and the micropore volume increased from 0.10 to 0.22 cm^3/g when the $SiO_2/P123$ molar ratios were increased from 59 to 152 (ageing temperature = 80 °C). Moreover, the increase of aging temperature has a negative influence on the micropore volume [16], and the micropore volume increased from 0.12 to 0.18 cm^3/g when the temperature was decreased from 100 to 80 °C ($SiO_2/P123 = 92$). These results can be further proved by the ratio of pore wall thickness to pore diameter, a criterion proposed by Vradman et al. [6] to confirm the microporosity in SBA-15, as listed in Table 1.

The pore ordering and morphology of HP_{59}-80, HP_{92}-80, HP_{125}-80 and HP_{152}-80 viewed in the direction perpendicular and parallel (inserts) to the pore axis were further examined with TEM, as shown in Fig. 3. All samples show typical hexagonal pore arrays

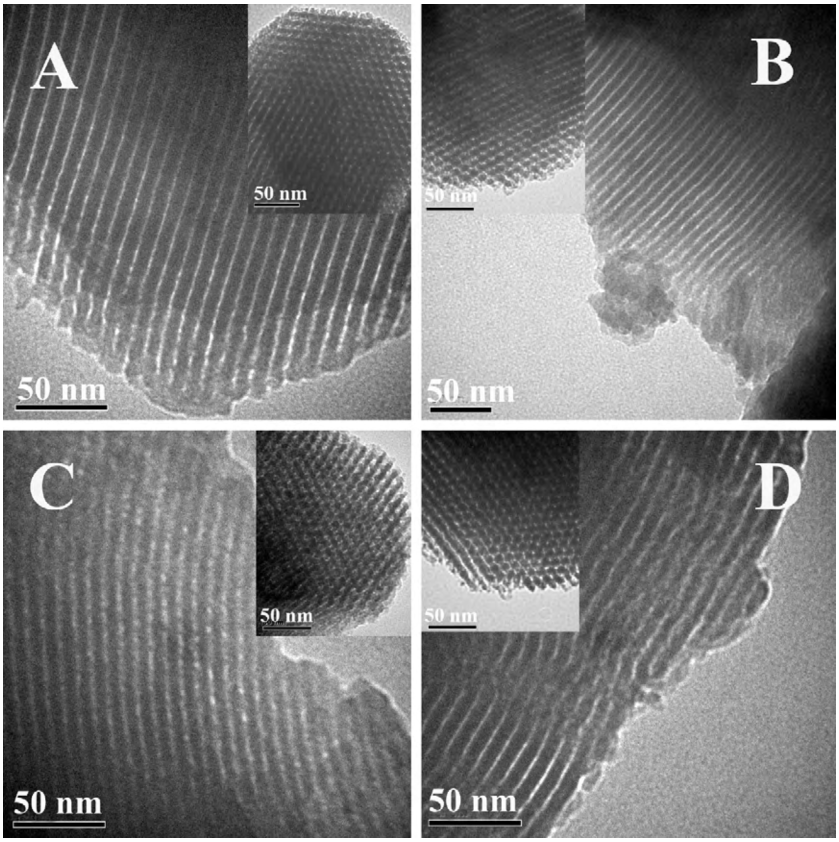

Fig. 3. TEM images of (a) HP_{59}-80, (b) HP_{92}-80, (c) HP_{125}-80 and (d) HP_{152}-80 viewed in the direction perpendicular and parallel (inserts) to the pore axis.

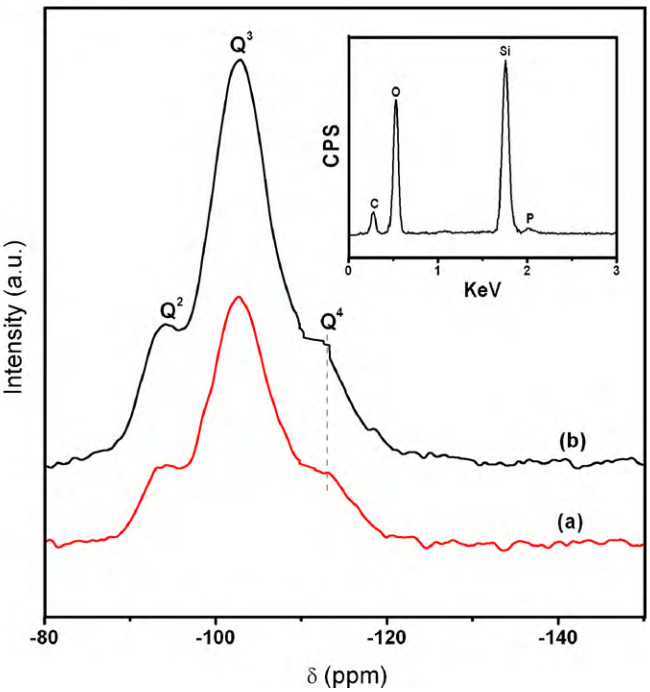

Fig. 4. ^{29}Si CP-MAS/NMR spectra of (a) HP_{59}-80 and (b) HP_{92}-80 (insert: EDS pattern of HP_{92}-80).

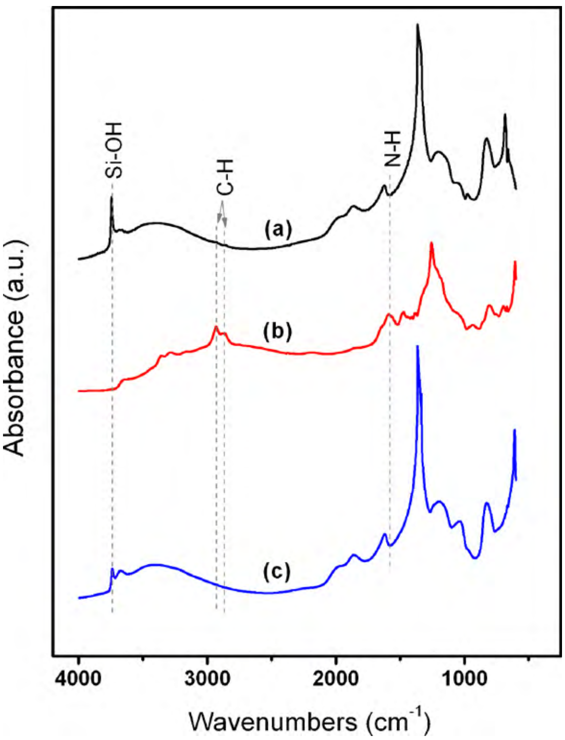

Fig. 5. FT-IR spectra of (a) HP_{92}-80, (b) A-HP_{92}-80 and (c) A-HP_{92}-80 (calcined).

and uniform straight pore channels, with a pore diameter in the range of *ca.* 5–7 nm, which is in well agreement with the results derived from the N_2 sorption (Fig. 2 and Table 1). Besides, it is worth noting that the long-range regularity of mesoporous array of HP_{125}-80 and HP_{152}-80 decreased to some extent (Fig. 3(c) and (d)), identical to the SA-XRD results, as shown in Fig. 1(g) and (h). The ^{29}Si cross-polarization magic-angle-spinning (CP-MAS)/NMR spectra of HP_{59}-80 and HP_{92}-80 were recorded to confirm the chemical nature of the silica framework, as shown in Fig. 4. ^{29}Si MAS NMR spectra display bands around −94 ppm (Q^2) and −103 ppm (Q^3), and these data are slightly shifted to negative values compared with pure SBA-15 (Q^2 = −92 ppm, Q^3 = −102 ppm), indicating that the phosphorus atoms are incorporated into the silica framework. In addition, the band appeared at approximately −114 ppm (Q^4) could be related to $Si(OSi)_{4-x}(OP)_x$ (x = 1–3) [13], suggesting that the phosphorus atoms would be cross-linked with the silicate matrix. On the other hand, the EDS analysis was performed to further confirm the presence of phosphorus atoms, and the experimental result reveals that the P content in HP_{92}-80 sample is about 1.04 wt.% (Fig. 4 (insert)). This result suggested that P atoms are incorporated into the silica matrix.

Fig. 5 displays the FT-IR spectra of HP_{92}-80, A-HP_{92}-80 and calcined A-HP_{92}-80 samples. Pure HP_{92}-80 material show characteristic bands at about 1632 and 3738 cm^{-1}, indicating the presence of stretching vibrations of isolated O–H bonds and Si–OH groups, respectively [34]. For A-HP_{92}-80, the peak at 3738 cm^{-1} disappeared, and three new infrared absorption bands at 1602, 2850 and 2900 cm^{-1} appeared. The absorption peak centered at 1602 cm^{-1} is attributed to the N–H asymmetric bending [35], and the peaks between 2700 and 2900 cm^{-1} can be assigned to the C–H stretching [36,37], indicating that the $–Si(CH_2)_3NH_2$ was created on the surface of HP_{92}-80 when the synthesized material was treated with APTMS. The characteristic absorption peaks at 1602, 2850 and 2900 cm^{-1} disappeared for the calcined A-HP_{92}-80 (550 °C for 2 h), indicating that the aminopropyl groups can be totally removed during the calcination process, as shown in Fig. 5(c). Fig. 6 shows the TG curves of HP_{92}-80 and A-HP_{92}-80 samples. The first weight loss below 140 °C was due to the desorption of physisorbed water, and the weights of the samples then slowly decreased up to about 290 °C due to the further desorption of water [38]. In addition, an obvious weight loss in the range of 290–550 °C can be observed in A-HP_{92}-80 (*ca.* 12.5 wt.%), while no evident weight loss occurs in HP_{92}-80, indicating the decomposition of functional groups ($–(CH_2)_3NH_2$). The small weight reduction between 550 and

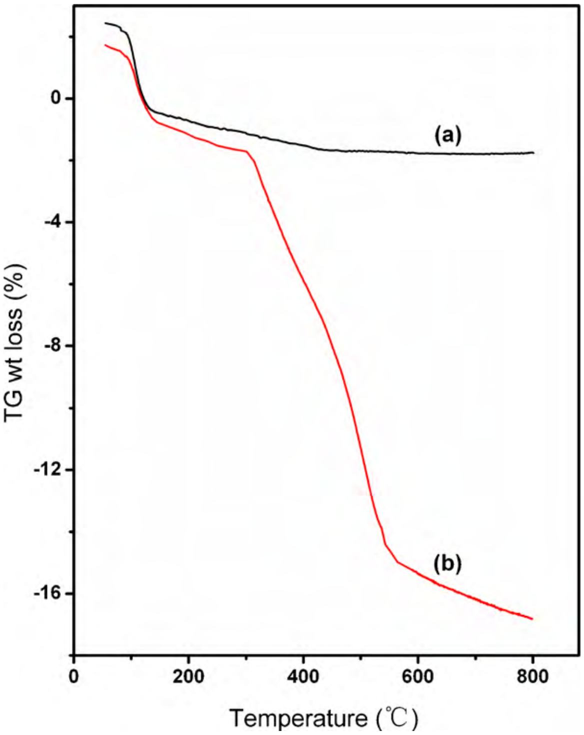

Fig. 6. Thermogravimetric analysis of (a) HP_{92}-80 and (b) A-HP_{92}-80.

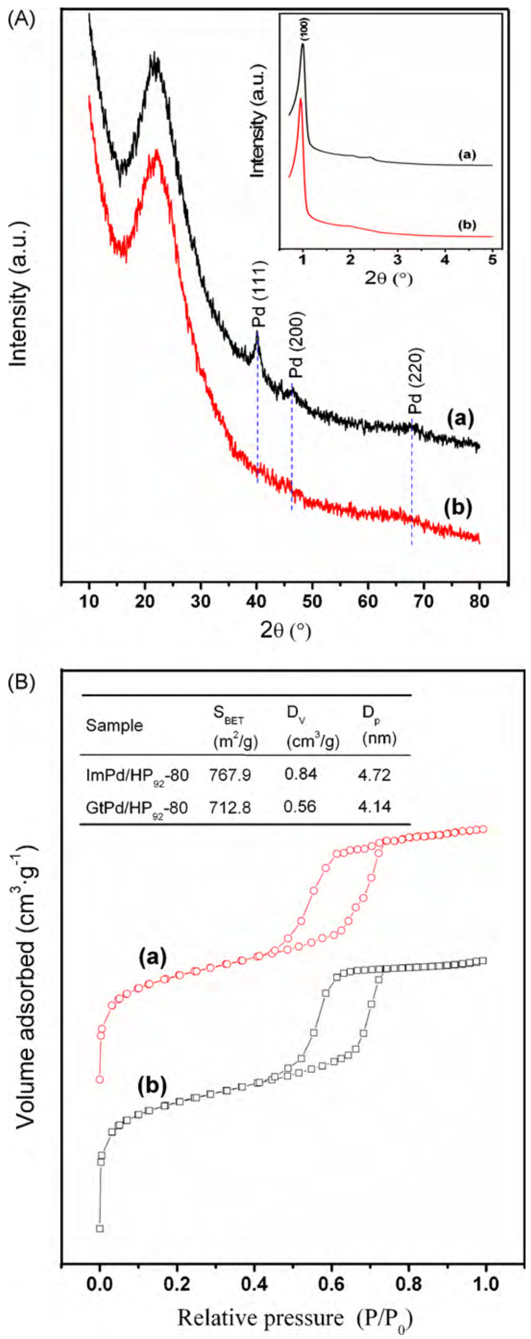

Sample	S_{BET} (m^2/g)	D_V (cm^3/g)	D_p (nm)
ImPd/HP$_{92}$-80	767.9	0.84	4.72
GtPd/HP$_{92}$-80	712.8	0.56	4.14

Fig. 7. (A) XRD patterns of (a) ImPd/HP$_{92}$-80 and (b) GtPd/HP$_{92}$-80 (inset: SA-XRD). (B) N_2 adsorption/desorption isotherms and physicochemical properties (insert table) of (a) GtPd/HP$_{92}$-80 and (b) ImPd/HP$_{92}$-80.

800 °C over A-HP$_{92}$-80 may be attributed to the release of water from condensation of silanols.

3.2. Structure analysis of Pd-supported catalysts

Fig. 7(A) shows the XRD patterns of ImPd/HP$_{92}$-80 and GtPd/HP$_{92}$-80 at low (insert) and high diffraction angles, respectively. The SA-XRD patterns reveal that the mesoporous structure of HP$_{92}$-80 is well sustained, suggesting that the Pd incorporation methods have insignificant influence on the support original structure. The wide-angle XRD patterns show that, at high diffraction angles (10–80°), the GtPd/HP$_{92}$-80 sample only has a broad diffraction peak at $2\theta \approx 23°$ ascribed to the amorphous silica [10]. However, for ImPd/HP$_{92}$-80, three new diffraction peaks appeared at $2\theta = 40.1°$, 46.4° and 68.2°, which can be assigned to (1 1 1), (2 0 0) and (2 2 0) reflections of metallic Pd, respectively (JCPDS: 46-1043). This suggests that relatively larger Pd particles were formed in ImPd/HP$_{92}$-80 sample. Fig. 7(B) displays the N_2 adsorption/desorption isotherms of ImPd/HP$_{92}$-80 and GtPd/HP$_{92}$-80, and the structure data (S_{BET}, D_v and D_p) are listed in the insert table. Both samples possess type IV isotherms (characteristic of mesoporous materials), indicating that the original mesoporous structure of HP$_{92}$-80 was well maintained during the catalyst synthesis procedures. Besides, comparing with pure HP$_{92}$-80, the D_v and D_p of ImPd/HP$_{92}$-80 just have a slight decrease, from 0.92 cm^3/g, and 4.76 nm, to 0.84 cm^3/g, and 4.72 nm, respectively. However, the D_v and D_p of GtPd/HP$_{92}$-80 decrease more significantly, from 0.92 cm^3/g, and 4.76 nm, to 0.56 cm^3/g, and 4.14 nm, respectively. A considerable decrease in the D_v and D_p indicated that the Pd atoms in the pore channels of GtPd/HP$_{92}$-80 are more than that of ImPd/HP$_{92}$-80 [39].

The typical TEM micrograph of ImPd/HP$_{92}$-80 and the representative HRTEM and STEM images of GtPd/HP$_{92}$-80 are shown in Fig. 8. First of all, the actual Pd loading in ImPd/HP$_{92}$-80 (ICP-OES: 2.01 wt.%) and GtPd/HP$_{92}$-80 (ICP-OES: 1.95 wt.%, EDS: 1.97 wt.%) is close to the nominal Pd content (2.0 wt.%), as shown in Fig. 8 and Table 2. The representative TEM, HRTEM and STEM images reveal that the synthesized catalysts have a well-ordered mesoporous channel structure, which supports the aforementioned SA-XRD and N_2 sorption results (Fig. 7). Spherical Pd nanoparticles with narrow distribution over ImPd/HP$_{92}$-80 sample (*ca.* 6–8 nm) are obviously larger than that of GtPd/HP$_{92}$-80 (*ca.* 1–3 nm), as shown in Fig. 8. Comparing with ImPd/HP$_{92}$-80, it is interesting to note that more Pd nanoparticles are located inside the mesoporous channels of GtPd/HP$_{92}$-80 (Fig. 8(A)–(C)). On the other hand, the dispersion of Pd atoms in the catalysts was further evaluated by H_2 chemisorption, as listed in Table 2. The results reveal that the Pd dispersion of GtPd/HP$_{92}$-80 (H/Pd = 0.54, D_c = 2.07 nm) is significantly higher than that of ImPd/HP$_{92}$-80 (H/Pd = 0.29, D_c = 3.86 nm), and this is in well agreement with the TEM observation results. It could be proposed that the amino groups dispersed on the HP$_{92}$-80 host surface chelated the Pd ions in stoichiometry. Therefore, the Pd ions would tend to be anchored homogeneously at the functionalized silica surface, and most of Pd nanoparticles formed upon calcination and reduction would be well dispersed on the host silica. While for traditional impregnation procedure, the $PdCl_2$ aqueous solution has some disadvantages in spreading over the hydrophobic silica surface [40], resulting in the poor dispersion of active phase. In order to directly observe the atomic structure of Pd nanoparticles over GtPd/HP$_{92}$-80 sample, the HRTEM analysis was performed, as displayed in Fig. 8(E). The result shows that the lattice fringes with d = 0.224 nm are clearly visible, which can be attributed to the (1 1 1) planes of metallic Pd.

3.3. Catalytic performance and stability of synthesized catalysts

During the toluene catalytic oxidation, the reaction products detected in the effluent are only CO_2, H_2O and trace CO, and no other organic byproducts can be detected. The light-off curves were used to compare the activity of the synthesized catalysts for toluene oxidation. Generally, the catalysts prepared by the grafting procedure possess higher toluene oxidation activities than that prepared by impregnation method, and GtPd/HP$_{92}$-80 has the highest activity, as shown in Fig. 9. The total conversion of toluene occurs at 249 °C for ImPd/HP$_{92}$-80. While for GtPd/HP$_{92}$-80, the conversion of toluene becomes appreciable at less than 150 °C, approaching 50% conversion of toluene at 187 °C, and quickly achieving complete conversion at 220 °C (Fig. 9). Considering the relatively high space velocity (45,000 h^{-1}) during the oxidation reactions, it seems

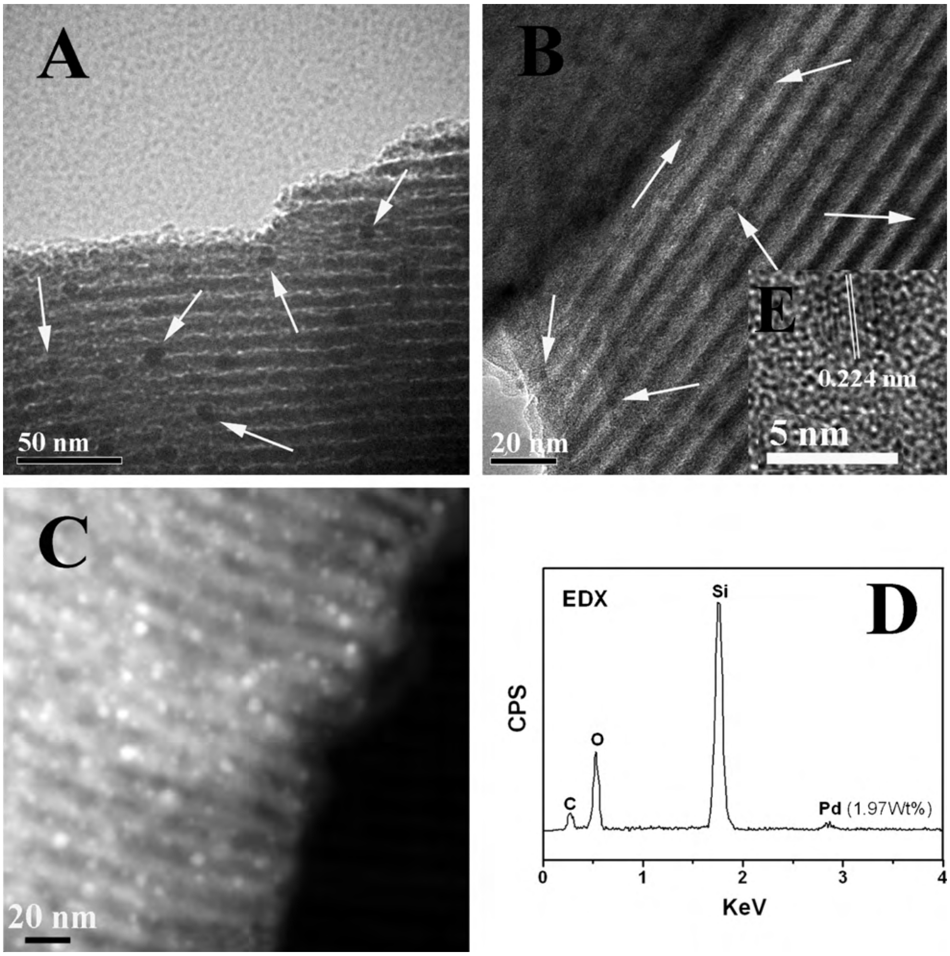

Fig. 8. (A) TEM image of ImPd/HP_{92}-80, (B-C) HRTEM and STEM images of GtPd/HP_{92}-80, (D) EDS result of GtPd/HP_{92}-80 and (E) HRTEM image of Pd nanoparticle confined in HP_{92}-80.

to be a good result of catalytic performance. Besides, the toluene oxidation activities of three selected catalysts (with various microporosity), i.e., GtPd/SBA-15, GtPd/HP_{59}-80 and GtPd/HP_{92}-80, were evaluated to explore the effect of microporosity on catalytic performance (Fig. 9). The experimental results indicate that the sample with higher micropore volume has superior catalytic activity, and the catalytic activity obeys the following order: GtPd/HP_{92}-80 > GtPd/HP_{59}-80 > GtPd/SBA-15. In this work, the CO_2 selectivity and yield (CO_2 selectivity (solid line); CO_2 yield (dashed line, calculated by (mole number of CO_2 produced)/7 × (mole number of toluene fed)) during toluene oxidation over ImPd/HP_{92}-80 and GtPd/HP_{92}-80 were further investigated, as shown in Fig. 10. It can be found that the gap between the toluene conversion and CO_2 yield for GtPd/HP_{92}-80 is much smaller than that of ImPd/HP_{92}-80, and the CO_2 yield of GtPd/HP_{92}-80 and ImPd/HP_{92}-80 can reach 100% at about 230 and 260 °C, respectively. Table 2 presents the toluene oxidation temperature (T_{10}, T_{50} and T_{90}) and CO_2 selectivity (S_{170}, S_{210} and S_{230}) over aforementioned catalysts. It is worth noting that the CO_2 selectivity of GtPd/HP_{92}-80 (98.3–100%) is higher than that of ImPd/HP_{92}-80 (90.6–100%) at different reaction temperatures. It is well known that a high activity of a supported catalyst often resulted from a large active surface area, i.e., a high dispersion of the active phase (small particle size) [41]. For GtPd/HP_{92}-80 sample, the Pd nanoparticles are well dispersed on the inner/outer surfaces of mesoporous SBA-15, which may result in the superior catalytic activity. While for ImPd/HP_{92}-80 sample, the impregnated palladium tends to agglomerate on the hydrophobic surface of SBA-15; thus the pore channels could be jammed to some extent, making the active sites in the intermediate position less accessible. In addition, a large number of micropores ($D_{mi} = 0.18\ cm^3/g$) within the primary pore wall of HP_{92}-80 could favor the smooth diffusion of reactant molecules to reach the active sites inside the pore channels and promote the desorption of products, and hence accelerate the toluene oxidation process.

Table 2
Characteristic data and catalytic results of synthesized catalysts.

Sample	Pd[a] (wt.%)	H/Pd[b]	D_c[c] (nm)	T_{10}[d] (°C)	T_{50}[d] (°C)	T_{90}[d] (°C)	S_{170}[e] (%)	S_{210}[e] (%)	S_{230}[e] (%)
ImPd/HP_{92}-80	2.01	0.29	3.86	173	195	225	92.6	95.8	97.5
GtPd/HP_{92}-80	1.95	0.54	2.07	164	187	210	100	99.7	100

[a] Actual Pd contents obtained by the ICP-OES analysis.
[b] Molar ratio of adsorbed hydrogen atoms to the total palladium atoms.
[c] Calculated diameters of the palladium crystallites based on the dispersion of Pd.
[d] Temperatures at which 10, 50 and 90% conversion of toluene.
[e] The CO_2 selectivity obtained at 170, 210 and 230 °C, respectively.

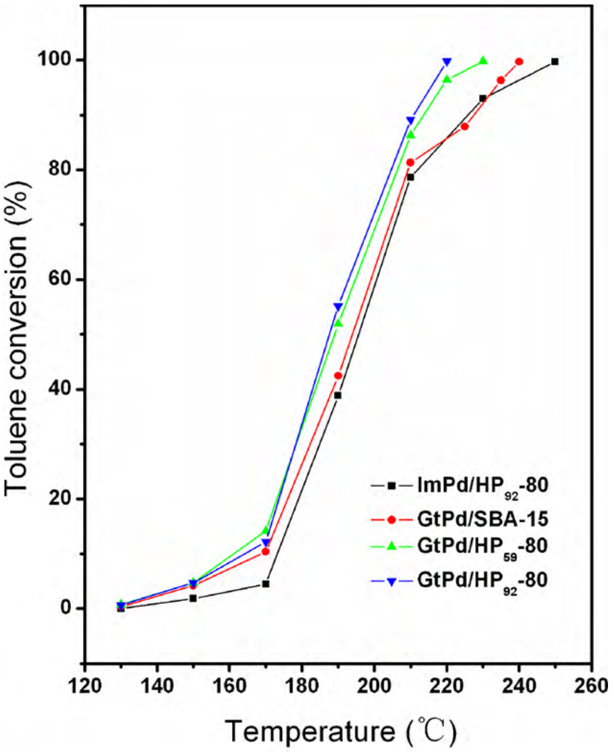

Fig. 9. Toluene oxidation over various Pd-loaded catalysts.

The stabilities of ImPd/HP$_{92}$-80 and GtPd/HP$_{92}$-80 were investigated for 50 h under conditions of 600 ppm of toluene in the feed gas, reaction temperature of 210 °C, and GHSV of 45,000 h^{-1}, as shown in Fig. 11. During the 50 h test, the toluene conversion over GtPd/HP$_{92}$-80 and ImPd/HP$_{92}$-80 is well maintained without noticeable activity loss. At the same time, it is worth to note that the CO_2 selectivity is also well sustained at 96 ± 2% (ImPd/HP$_{92}$-80) and 99 ± 1% (GtPd/HP$_{92}$-80), indicating that the catalytic performance of both catalysts is well sustained. Besides, the Pd contents in used ImPd/HP$_{92}$-80 (1.98 wt.%) and GtPd/HP$_{92}$-80 (1.96 wt.%) are close to the nominal Pd loading, indicating that no palladium leaches from the support during the stability test. As a consequence, these catalysts should be promising materials for VOCs elimination.

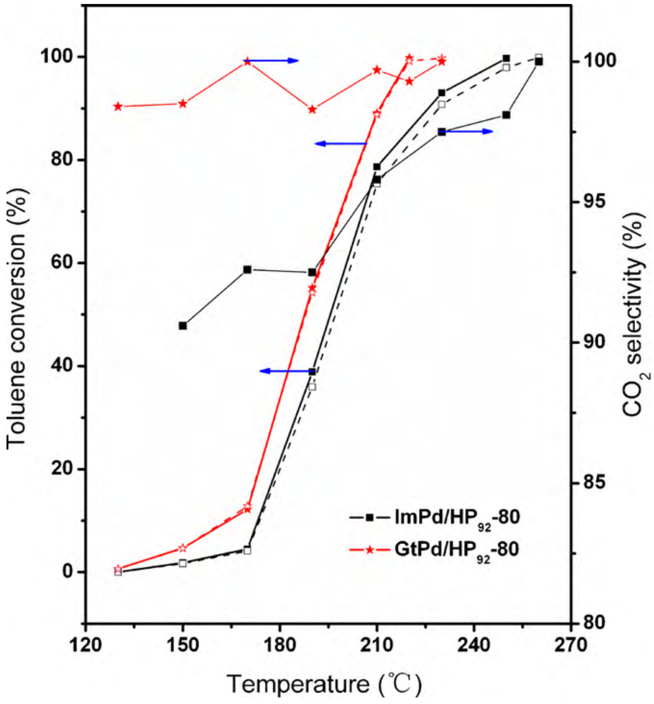

Fig. 10. Conversion and selectivity profiles of toluene oxidation over Pd-loaded catalysts.

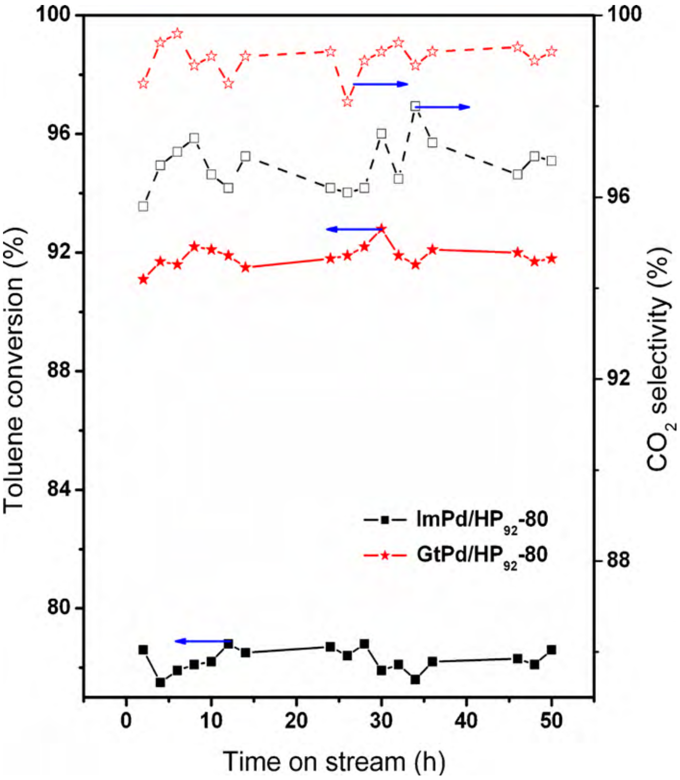

Fig. 11. Stability investigations for toluene combustion with time-on-stream over ImPd/HP$_{92}$-80 and GtPd/HP$_{92}$-80.

4. Conclusions

The mesoporous SBA-15 with increased surface area and enhanced micropore volume were successfully synthesized through a simple and effective approach. It was found that the addition of H_3PO_4 during the template formation process produced an obvious increase in the surface area of the obtained materials, and the micropore volume can be systematically controlled by the SiO_2/P123 ratio and synthesis temperature, and these biporous materials should exhibit extraordinary performance in catalysis, adsorption, and separation.

We also further functionalized the SBA-15 by grafting Pd nanoparticles for formulating the catalysis. Compared with impregnation method, the grafting procedure appears more promising in designing highly dispersed Pd particles on the silica-based mesoporous materials. The catalyst prepared *via* the grafting procedure catalyzes the toluene far more effectively (with much higher activity and selectivity) than that prepared by impregnation method. Both the synthesized catalysts show a good long-term stability and the toluene conversion and CO_2 selectivity can be well maintained during 50 h tests. Thus, these catalysts are effective and promising materials in the elimination of VOCs.

Acknowledgements

National Basic Research Program of China (No. 2010CB732300), the National High Technology Research and Development Program of China (No. 2006AA06A310), and National Science Fund for Distinguished Young Scholars (No. 20725723) are gratefully acknowledged.

References

[1] Q. Hu, J.J. Li, Z.P. Hao, L.D. Li, S.Z. Qiao, Dynamic adsorption of volatile organic compounds on organofunctionalized SBA-15 materials, Chem. Eng. J. 149 (2009) 281–288.

[2] C. He, J.J. Li, J. Cheng, L.D. Li, P. Li, Z.P. Hao, Z.P. Xu, Comparative studies on porous material-supported Pd catalysts for catalytic oxidation of benzene, toluene, and ethyl acetate, Ind. Eng. Chem. Res. 48 (2009) 6930–6936.

[3] X.H. Wang, T.H. Sun, J. Yang, L. Zhao, J.P. Jia, Low-temperature H_2S removal from gas streams with SBA-15 supported ZnO nanoparticles, Chem. Eng. J. 142 (2008) 48–55.

[4] K. Miyazawa, S. Inagaki, Control of the microporosity within the pore walls of ordered mesoporous silica SBA-15, Chem. Commun. 22 (2000) 2121–2122.

[5] P.D. Yang, D.Y. Zhao, D.I. Margolese, B.F. Chmelka, G.D. Stucky, Generalized syntheses of large-pore mesoporous metal oxides with semicrystalline frameworks, Nature 396 (1998) 152–155.

[6] L. Vradman, L. Titelman, M. Herskowitz, Size effect on SBA-15 microporosity, Micropor. Mesopor. Mater. 93 (2006) 313–317.

[7] F.Q. Zhang, Y. Yan, H.F. Yang, Y. Meng, C.Z. Yu, B. Tu, D.Y. Zhao, Understanding effect of wall structure on the hydrothermal stability of mesostructured silica SBA-15, J. Phys. Chem. B 109 (2005) 8723–8732.

[8] Y.F. Han, F.X. Chen, Z.Y. Zhong, K. Ramesh, L.W. Chen, D. Jian, W.W. Ling, Complete oxidation of low concentration ethanol in aqueous solution with H_2O_2 on nanosized Mn_3O_4/SBA-15 catalyst, Chem. Eng. J. 134 (2007) 276–281.

[9] J. Aguado, G. Callej, A. Carrero, J. Moreno, One-step synthesis of chromium and aluminium containing SBA-15 materials—New phillips catalysts for ethylene polymerization, Chem. Eng. J. 137 (2008) 443–452.

[10] Z.J. Wang, Y.B. Xie, C.J. Liu, Synthesis and characterization of noble metal (Pd, Pt, Au, Ag) nanostructured materials confined in the channels of mesoporous SBA-15, J. Phys. Chem. C 112 (2008) 19818–19824.

[11] P.F. Fulvio, S. Pikus, M. Jaroniec, SBA-15-supported mixed-metal oxides: partial hydrolytic sol-gel synthesis, adsorption, and structural properties, ACS Appl. Mater. Interfaces 2 (2010) 134–142.

[12] P. Van Der Voort, P.I. Ravikovitch, K.P. De Jong, M. Benjelloun, E. Van Bavel, A.H. Janssen, A.V. Neimark, B.M. Weckhuysen, E.F. Vansant, A new templated ordered structure with combined micro- and mesopores and internal silica nanocapsules, J. Phys. Chem. B 106 (2002) 5873–5877.

[13] M. Colilla, F. Balas, M. Manzano, M. Vallet-Regi, Novel method to enlarge the surface area of SBA-15, Chem. Mater. 19 (2007) 3099–3101.

[14] J.M. Herrera, J. Reyes, P. Roquero, T. Kimova, New hydrotreating NiMo catalysts supported on MCM-41 modified with phosphorus, Micropor. Mesopor. Mater. 83 (2005) 283–291.

[15] M. Vallet-Regi, L. Ruiz-González, I. Lzquierdo-Barba, J.M. González-Calbet, Revisiting silica based ordered mesoporous materials: medical applications, J. Mater. Chem. 16 (2006) 26–31.

[16] M. Kruk, M. Jaroniec, C.H. Ko, R. Ryoo, Characterization of the porous structure of SBA-15, Chem. Mater. 12 (2000) 1961–1968.

[17] N. Li, F. Gaillard, Catalytic combustion of toluene over electrochemically promoted Ag catalyst, Appl. Catal. B: Environ. 88 (2009) 152–159.

[18] S.F. Zuo, Q.Q. Huang, J. Li, R.X. Zhou, Promoting effect of Ce added to metal oxide supported on Al pillared clays for deep benzene oxidation, Appl. Catal. B: Environ. 91 (2009) 204–209.

[19] C. He, P. Li, J. Cheng, Z.P. Hao, Z.-P. Xu, A comprehensive study of deep catalytic oxidation of benzene, toluene, ethyl acetate, and their mixtures over Pd/ZSM-5 catalyst: mutual effects and kinetics, Water Air Soil Pollut. 209 (2010) 365–376.

[20] T. Williams, J. Beltramini, G.Q. Lu, Effect of the preparation technique on the catalytic properties of mesoporous V-HMS for the oxidation of toluene, Micropor. Mesopor. Mater. 88 (2006) 91–100.

[21] C. He, J.J. Li, P. Li, J. Cheng, Z.P. Hao, Z.-P. Xu, Comprehensive investigation of Pd/ZSM-5/MCM-48 composite catalysts with enhanced activity and stability for benzene oxidation, Appl. Catal. B: Environ. 96 (2010) 466–475.

[22] W.G. Shim, J.W. Lee, S.C. Kim, Analysis of catalytic oxidation of aromatic hydrocarbons over supported palladium catalyst with different pretreatments based on heterogeneous adsorption properties, Appl. Catal. B: Environ. 84 (2008) 133–141.

[23] S.C. Kim, W.G. Shim, Properties and performance of Pd based catalysts for catalytic oxidation of volatile organic compounds, Appl. Catal. B: Environ. 92 (2009) 429–436.

[24] C. He, P. Li, J. Cheng, J.J. Li, Z.P. Hao, Preparation and investigation of Pd/Ti-SBA-15 catalysts for catalytic oxidation of benzene, Environ. Prog. Sust. Energy (2009), doi:10. 1002/ep.10427.

[25] D. Zhao, J. Feng, Q. Huo, N. Melosh, G.H. Fredrickson, B.F. Chemlkav, G.D. Stucky, Triblock copolymer syntheses of mesoporous silica with periodic 50 to 300 angstrom pores, Science 279 (1998) 548–552.

[26] N. Krishnankutty, J. Li, M.A. Vannice, The effect of Pd precursor and pretreatment on the adsorption and absorption behavior of supported Pd catalysts, Appl. Catal. A: Gen. 173 (1998) 137–144.

[27] C. He, P. Li, J. Cheng, H.L. Wang, J.J. Li, Q. Li, Z.P. Hao, Synthesis and characterization of Pd/ZSM-5/MCM-48 biporous catalysts with superior activity for benzene oxidation, Appl. Catal. A: Gen. (2010), doi:10.1016/j.apcata.2010.04.033.

[28] A. Galarneau, H. Cambon, F.D. Renzo, F. Fajula, True microporosity and surface area of mesoporous SBA-15 silicas as a function of synthesis temperature, Langmuir 17 (2001) 8328–8335.

[29] J. Zhu, Z. Kónya, V.F. Puntes, I. Kiricsi, C.X. Miao, J.W. Ager, A.P. Alivisatos, G.A. Somorjai, Encapsulation of metal (Au, Ag, Pt) nanoparticles into the mesoporous SBA-15 structure, Langmuir 19 (2003) 4396–4401.

[30] K.S.W. Sing, D.H. Everett, R.A.W. Haul, L. Moscou, R.A. Pierotti, J. Rouquérol, T. Siemieniewska, Reporting physisorption data for gas/solid systems with special reference to the determination of surface area and porosity, Pure Appl. Chem. 57 (1985) 603–619.

[31] C.M. Yang, B. Zibrowius, W. Schmidt, F. Schüth, Stepwise removal of the copolymer template from mesopores and micropores in SBA-15, Chem. Mater. 16 (2004) 2918–2925.

[32] S. Ruthstein, J. Schmidt, E. Kesselman, Y. Talmon, D. Goldfarb, Resolving intermediate solution structure during the formation of mesoporous SBA-15, J. Am. Chem. Soc. 128 (2006) 3366–3374.

[33] R.K. Iler, The Chemistry of Silica, Wiley-Interscience, New York, 1979.

[34] P. Han, H.M. Zhang, X.P. Qiu, X.L. Ji, L.X. Gao, Palladium within ionic liquid functionalized mesoporous silica SBA-15 and its catalytic application in room-temperature Suzuki coupling reaction, J. Mol. Catal. A: Chem. 295 (2008 295 57-67).

[35] S.W. Song, K. Hidajat, S. Kawi, Functionalized SBA-15 materials as carriers for controlled drug delivery: influence of surface properties on matrix-drug interactions, Langmuir 21 (2005) 9568–9575.

[36] S. Fiorolli, B. Onida, C. Barolo, G. Viscardi, D. Brunel, E. Garrone, Tethering of modified reichardt's dye on SBA-15 mesoporous silica: the effect of the linker flexibility, Langmuir 23 (2007) 2261–2268.

[37] C. He, P. Li, J.J. Li, H.L. Wang, J. Cheng, X.Y. Zhang, Z.P. Hao, Ligand-assisted preparation of highly active and stable nanometric Pd confined catalysts for deep catalytic oxidation of toluene, J. Hazard. Mater. (2010), doi:10.1016/j.jhazmat.2010.05.113.

[38] B. Lee, Y. Kim, H. Lee, J. Yi, Synthesis of functionalized porous silicas via templating method as heavy metal ion adsorbents: the introduction of surface hydrophilicity onto the surface of adsorbents, Micropor. Mesopor. Mater. 50 (2001) 77–90.

[39] S.-C. Chang, M.H. Huang, Formation of short In_2O_3 nanorod arrays within mesoporous silica, J. Phys. Chem. C 112 (2008) 2304–2307.

[40] J.J. Li, X.Y. Xu, Z. Jiang, Z.P. Hao, C. Hu, Nanoporous silica-supported nanometric palladium: synthesis, characterization, and catalytic deep oxidation of benzene, Environ. Sci. Technol. 39 (2005) 1319–1323.

[41] S. Lambert, C. Cellier, E.M. Gaigneaux, J.-P. Pirard, B. Heinrichs, Ag/SiO_2, Cu/SiO_2 and Pd/SiO_2 cogelled xerogel catalysts for benzene combustion: Relationships between operating synthesis variables and catalytic activity, Catal. Commun. 8 (2007) 1244–1248.